Cell Reports

PF4 Promotes Platelet Production and Lung Cancer Growth

Graphical Abstract

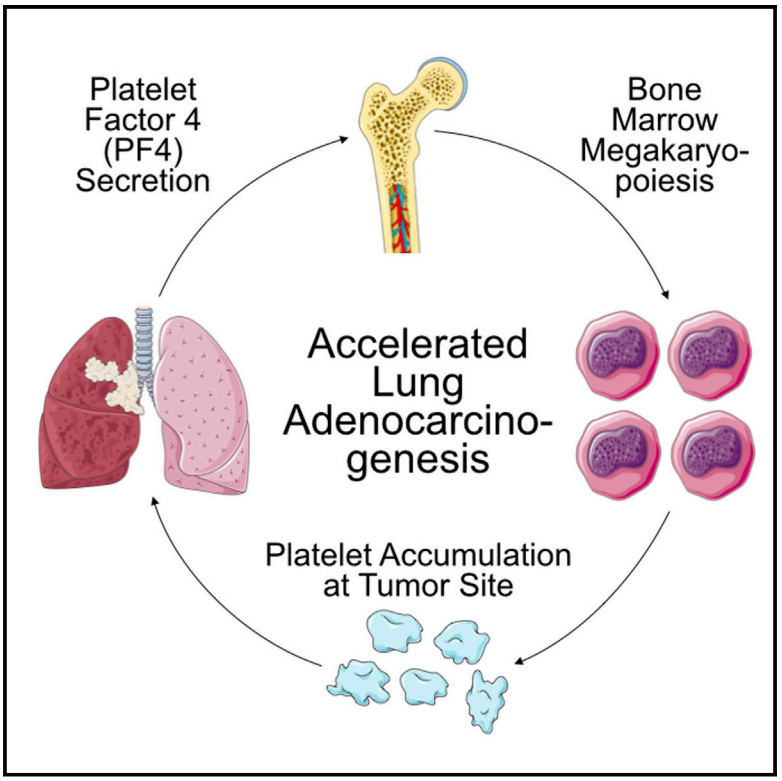

Highlights

- PF4 overexpression is associated with altered lung cancer patient survival
- PF4 induces megakaryopoiesis in lung tumor-bearing mice
- PF4 increases platelet accumulation in tumor-bearing lungs
- Platelets and PF4 promote lung adenocarcinogenesis in mice

Authors

Ferdinando Pucci, Steffen Rickelt, Andita P. Newton, ..., Richard O. Hynes, Ralph Weissleder, Mikael J. Pittet

Correspondence

mpittet@mgh.harvard.edu

In Brief

Tumors can act over extended distances to stimulate tumor-promoting immune responses, but the long-range signals involved remain poorly understood. Pucci et al. now suggest that platelet factor 4 (PF4) can stimulate bone marrow megakaryopoiesis and lung cancer progression.

Pucci et al., 2016, Cell Reports *17*, 1764–1772
November 8, 2016
http://dx.doi.org/10.1016/j.celrep.2016.10.031

CellPress

OPEN ACCESS
CellPress

Cell Reports
Report

PF4 Promotes Platelet Production and Lung Cancer Growth

Ferdinando Pucci,[1,8] Steffen Rickelt,[2] Andita P. Newton,[1] Christopher Garris,[1,3] Ernesto Nunes,[4] Charles Evavold,[1,3] Christina Pfirschke,[1] Camilla Engblom,[1,3] Mari Mino-Kenudson,[5] Richard O. Hynes,[2] Ralph Weissleder,[1,6,7] and Mikael J. Pittet[1,6,9,*]

[1]Center for Systems Biology, Massachusetts General Hospital Research Institute, Harvard Medical School, Boston, MA 02114, USA
[2]Howard Hughes Medical Institute, Koch Institute for Integrative Cancer Research, Massachusetts Institute of Technology, Cambridge, MA 02139, USA
[3]Graduate Program in Immunology, Harvard Medical School, Boston, MA 02115, USA
[4]Department of Computer Science and Engineering, University of Minnesota, Minneapolis, MN 55455, USA
[5]Department of Pathology, Massachusetts General Hospital, Boston, MA 02114, USA
[6]Department of Radiology, Massachusetts General Hospital, Boston, MA 02114, USA
[7]Department of Systems Biology, Harvard Medical School, MA 02115, USA
[8]Present address: Torque Therapeutics Inc., Cambridge, MA 02142, USA
[9]Lead Contact
*Correspondence: mpittet@mgh.harvard.edu
http://dx.doi.org/10.1016/j.celrep.2016.10.031

SUMMARY

Co-option of host components by solid tumors facilitates cancer progression and can occur in both local tumor microenvironments and remote locations. At present, the signals involved in long-distance communication remain insufficiently understood. Here, we identify platelet factor 4 (PF4, CXCL4) as an endocrine factor whose overexpression in tumors correlates with decreased overall patient survival. Furthermore, engineered PF4 over-production in a Kras-driven lung adenocarcinoma genetic mouse model expanded megakaryopoiesis in bone marrow, augmented platelet accumulation in lungs, and accelerated de novo adenocarcinogenesis. Additionally, anti-platelet treatment controlled mouse lung cancer progression, further suggesting that platelets can modulate the tumor microenvironment to accelerate tumor outgrowth. These findings support PF4 as a cancer-enhancing endocrine signal that controls discrete aspects of bone marrow hematopoiesis and tumor microenvironment and that should be considered as a molecular target in anticancer therapy.

INTRODUCTION

Diverse tumor-associated host cells, including endothelial cells, fibroblasts, and hematopoietic cells, are often locally co-opted by tumors to enable tumorigenesis or sustain tumor outgrowth (Hanahan and Coussens, 2012; Engblom et al., 2016). The study of the cellular and molecular mechanisms underlying the tumor microenvironment has generated not only new anticancer treatments, such as immuno- and antiangiogenic therapies, but also a new field of fundamental investigation centered on the ontogeny of tumor-infiltrating host cells (McAllister and Weinberg, 2014; Pittet et al., 2014). This research has discovered that growing tumors can continuously recruit new hematopoietic cells from the circulation by releasing signals that amplify the production of hematopoietic progenitors in remote hematopoietic organs. Long-range tumor-associated signals include osteopontin, a tumor-secreted endocrine factor that activates bone marrow cells (McAllister et al., 2008); G-CSF, a tumor-derived factor that promotes bone marrow myelopoiesis (Casbon et al., 2015); and Angiotensin-II, a peptide hormone that instigates extramedullary monocytopoiesis (Cortez-Retamozo et al., 2013). However, while local immune-neoplastic interactions in the microenvironment are well studied, several aspects of systemically activated tumor-associated immune components remain unclear.

Here we aimed to identify new candidate long-range communication signals involved in lung adenocarcinoma. We focused on this disease because it is the leading cause of cancer death (Torre et al., 2016) and because newly available high-throughput datasets allowed us to interrogate this disease in both patients (Nguyen et al., 2009) and genetic mouse models that closely recapitulate the human disease (Taguchi et al., 2011). Initially, we developed a screening strategy that considered the following three defining properties of tumor-associated endocrine factors: (1) their expression in tumors should be altered in both murine and human lung adenocarcinomas, (2) their changed expression should be associated with differences in patient survival, and (3) their plasma concentration should be modified in lung adenocarcinoma-bearing mice. Interrogating these phenotypes in both humans and mice enabled us to identify circulating factors that may be relevant to human disease and that can be manipulated genetically to allow murine analyses of mechanisms and causality.

This strategy identified several factors and, of these, platelet factor 4 (PF4) seemed the most prominent in lung cancer. We

next performed deeper biological studies to identify whether systemically overexpressed PF4 instigates hematopoietic cell production away from the tumor stroma, instructs differentiation of defined hematopoietic cell types, and alters the tumor microenvironment and tumorigenesis. To this end, we compared lung adenocarcinoma genetic mouse models that expressed *Pf4* at either low or high levels, and we genetically induced systemic PF4 production in mice that otherwise expressed this factor at low levels. In doing so, we found PF4 to be responsible for stimulating discrete tumor-induced changes, namely megakaryocytic expansion in bone marrow and platelet accumulation at the tumor site. Furthermore, systemic PF4 production substantially accelerated Kras-driven tumorigenesis, a result that supports this factor as a tumor-promoting signal that connects lung tumors to distinct bone-marrow hematopoietic components.

RESULTS

Identification of Candidate Long-Range Factors Associated with Altered Patient Survival

To identify previously unknown long-range communication signals involved in lung adenocarcinoma, we screened in silico candidate long-range factors in Kras lung adenocarcinoma-bearing mice (Taguchi et al., 2011) and lung adenocarcinoma patients (Nguyen et al., 2009) (Figure 1A). By considering plasma proteins with significantly varied expression ($p < 0.05$) in tumor-bearing mice, when compared to tumor-free littermates (Taguchi et al., 2011), we short-listed 60 candidate factors, of which 33 were over-abundant and 27 were under-abundant (Figure S1A).

To assess these 60 factors in lung adenocarcinoma patients, we mined both tumor transcriptome profiles (at time of diagnosis) and survival data from 225 patients (Nguyen et al., 2009). Specifically, we compared the overall patient survival with highest (top 20%) and lowest (bottom 20%) mRNA expression levels for each candidate factor. Of the 33 over-abundant factors noted above, six were associated with altered patient survival ($p < 0.05$ after Bonferroni correction): overexpression of three of them (*Pf4*, *Agt*, and *Ppia*) correlated with decreased patient survival, while overexpression of the remaining three (*Npc2*, *Sftpb*, and *Slit2*) correlated with increased patient survival (Figure 1B). Of the 27 under-abundant factors noted above, five were associated with altered patient survival: under-expression of four of them (*Prg4*, *Rgn*, *Sepp1*, and *Thumpd1*) correlated with decreased patient survival while under-expression of *Wdr62* correlated with increased patient survival (Figure 1C). Overall, this screening identified four candidate harmful factors (*Pf4*, *Agt*, *Ppia*, and *Wdr62*) and seven candidate protective factors (*Npc2*, *Prg4*, *Rgn*, *Sepp1*, *Sftpb*, *Slit2*, and *Thumpd1*) in lung adenocarcinoma. Thus, 11 of the initial 60 candidates were associated with altered overall patient survival. For comparison, when assessing 60 randomly selected genes, we found that only 2.6 ± 0.2 (mean ± SEM, n = 60 iterations) of them were associated with differences in patient survival. Consequently, seeding our screening with cancer-associated endocrine factors significantly increased the chance that such candidates also were associated with survival changes (11 compared to 2.6 ± 0.2; $p < 0.0001$).

To further test the harmful and protective candidate factors identified above, we evaluated whether their transcript levels were altered at the tumor site in lung adenocarcinoma models driven by either oncogenic Kras only ($Kras^{G12D}$, hereafter referred to as K) or oncogenic Kras and p53 deletion ($Kras^{G12D}$;$p53^{fl/fl}$, hereafter referred to as KP). We used these two genetic models because they both carry mutations frequently found in human lung adenocarcinoma (*KRAS* and *TP53* are mutated in ~25% and ~50% of patients, respectively) but may co-opt the host immune response differently and produce different protective and harmful factors. Cre-expressing adenoviruses were introduced intranasally into K or KP mice to enable Cre delivery to lung epithelial cells and allow tumors to arise in the tissue (DuPage et al., 2009). We assayed intratumoral mRNA expression levels when tumor burden was similar in both models (Figure S1B), i.e., at week 20 for K mice and at week 11 for KP mice. Our assay also included tumor-free lungs as control tissue. Two of seven harmful candidate genes (*Pf4* and *Agt*) and two of four protective candidate genes (*Npc2* and *Sftpb*) were significantly overexpressed in KP tumors; *Sftpb* also was overexpressed in K tumors (Figure 1D). The candidate protective factor *Prg4* was under-expressed in K mice (Figure 1E).

PF4 as a Candidate Lung Adenocarcinoma-Promoting Factor

Of the harmful candidate factors identified above, we sought to further interrogate PF4 because it was most highly (~30-fold) overexpressed in KP nodules when compared to K nodules and tumor-free lungs (Figure 1D). Also, PF4 levels in circulation and within tumors have been associated with increased tumor growth (Poruk et al., 2010), but whether PF4 causally affects tumor development has remained unknown. Additionally, defining whether and how PF4 impacts distant organs and/or plays a role in tumor-host communication required study. Our initial data indicated a strong association between *PF4* overexpression and tumor development based on increased circulating PF4 plasma levels in Kras-driven lung tumor models (Figure S1A) and decreased overall survival in patients with high *PF4* expression in tumor nodules (Figure 1B). The latter finding was confirmed using independent lung adenocarcinoma datasets from 665 patients (Shedden et al., 2008) (Figure S1C). Also, statistical analysis of demographic data from the two cohorts of patients identified based on *PF4* expression levels in tumors (i.e., $PF4^{HI}$ and $PF4^{LO}$ patients) did not identify a bias that could explain the underlying difference in survival (Figure S1D).

In subsequent experiments, we genetically augmented systemic PF4 production in K mice, which were otherwise poor *Pf4* expressers (Figure 1D), and we asked whether this change was sufficient to induce discrete alterations in hematopoietic tissues and the tumor microenvironment that could foster tumor progression. To increase systemic PF4 levels in K mice, we created a lentiviral vector (PF4-LV) containing the native murine *Pf4* coding sequence under the strong constitutive promoter/enhancer *hEF1a* (Figure 2A), and we injected concentrated PF4-LV preparations intravenously (i.v.) to transduce liver cells in vivo. An LV lacking the *Pf4* expression cassette was used as a control (Ctrl-LV) (Figure S2A). We excluded marker genes in both vectors to avoid immune clearance of transduced cells

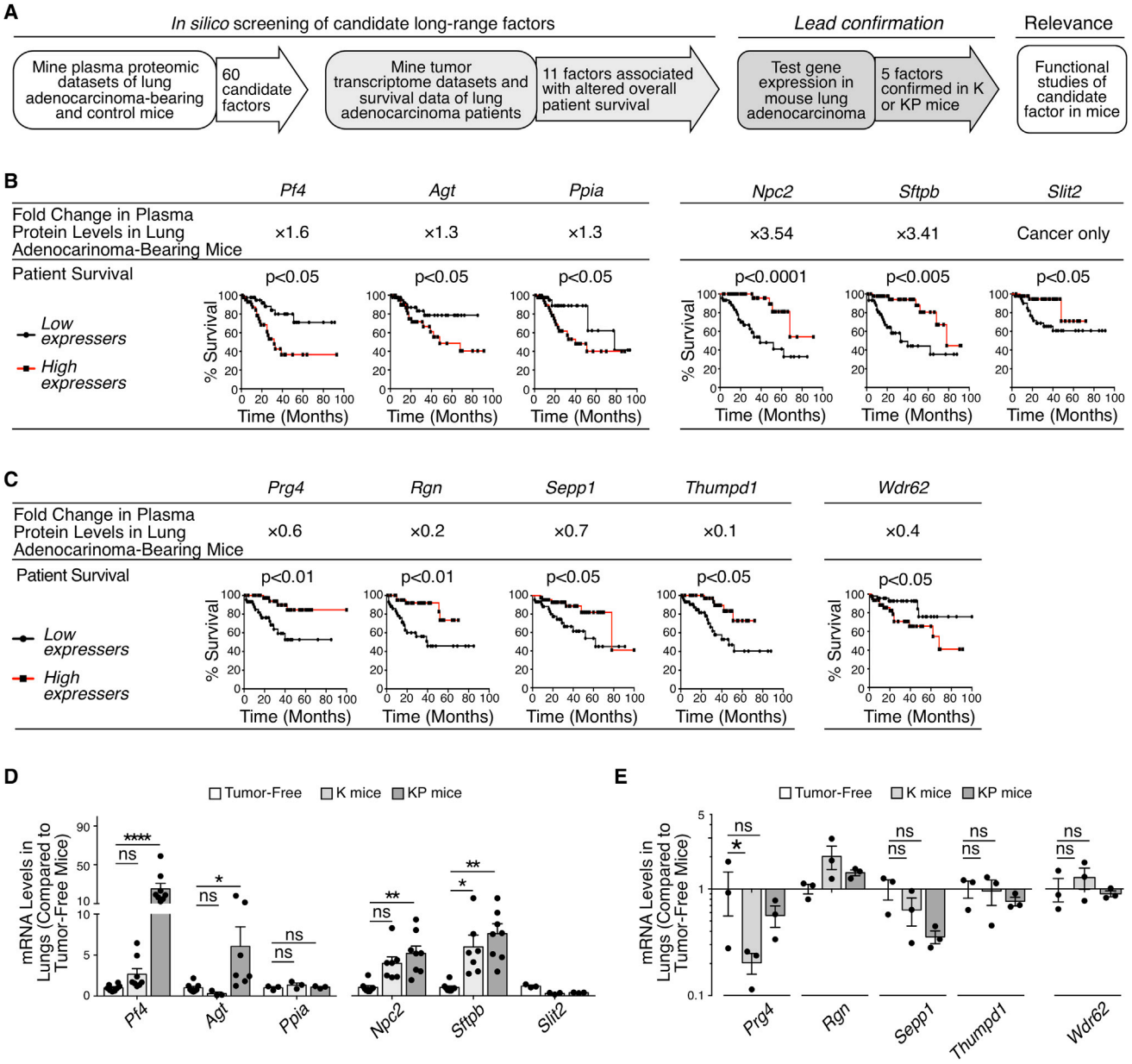

Figure 1. PF4 Is a Candidate Long-Range Factor Associated with Altered Survival in Lung Adenocarcinoma

(A) Workflow to identify candidate long-range endocrine signals involved in lung adenocarcinoma progression. The in silico screening employed a mouse proteomic dataset that cross-referenced a list of 60 candidate factors with patient microarray data to short-list 11 factors associated with altered patient survival (left panels). Leads were tested experimentally in K and KP mice (middle panels), and one factor was selected for further functional studies (right panel).

(B) Identification of six factors over-abundant in plasma of lung adenocarcinoma-bearing mice as compared to tumor-free mice (top row) and whose over-expression was associated with decreased (Pf4, Agt, and Ppia) or increased (Npc2, Sftpb, and Slit) survival in lung adenocarcinoma patients (bottom row). Kaplan-Meier survival curves are shown for patients with highest (top 20%, n = 45) and lowest (bottom 20%, n = 45) mRNA expression levels for each factor.

(C) Identification of five factors under-abundant in plasma of lung adenocarcinoma-bearing mice as compared to tumor-free mice (top row) and whose over-expression was associated with increased (Prg4, Rgn, Sepp1, and Thumpd1) or decreased (Wdr62) survival in lung adenocarcinoma patients (bottom row). Kaplan-Meier survival curves are shown for patients with highest (top 20%, n = 45) and lowest (bottom 20%, n = 45) mRNA expression levels for each factor.

(D and E) mRNA levels in K and KP mouse lungs (as compared to tumor-free lungs) when tumor burden was similar in both models, i.e., at week 20 for K mice and at week 11 for KP mice. Candidate factors from (B) and (C) are shown in (D) and (E), respectively (n = 3–8).

Results are expressed as mean ± SEM (*p < 0.05, **p < 0.01, and ****p < 0.0001). Abbreviations are as follows: K, $Kras^{G12D}$; KP, $Kras^{G12D}$;$p53^{fl/fl}$; ns, not significant; NSCLC, non-small-cell lung cancer. See also Figure S1.

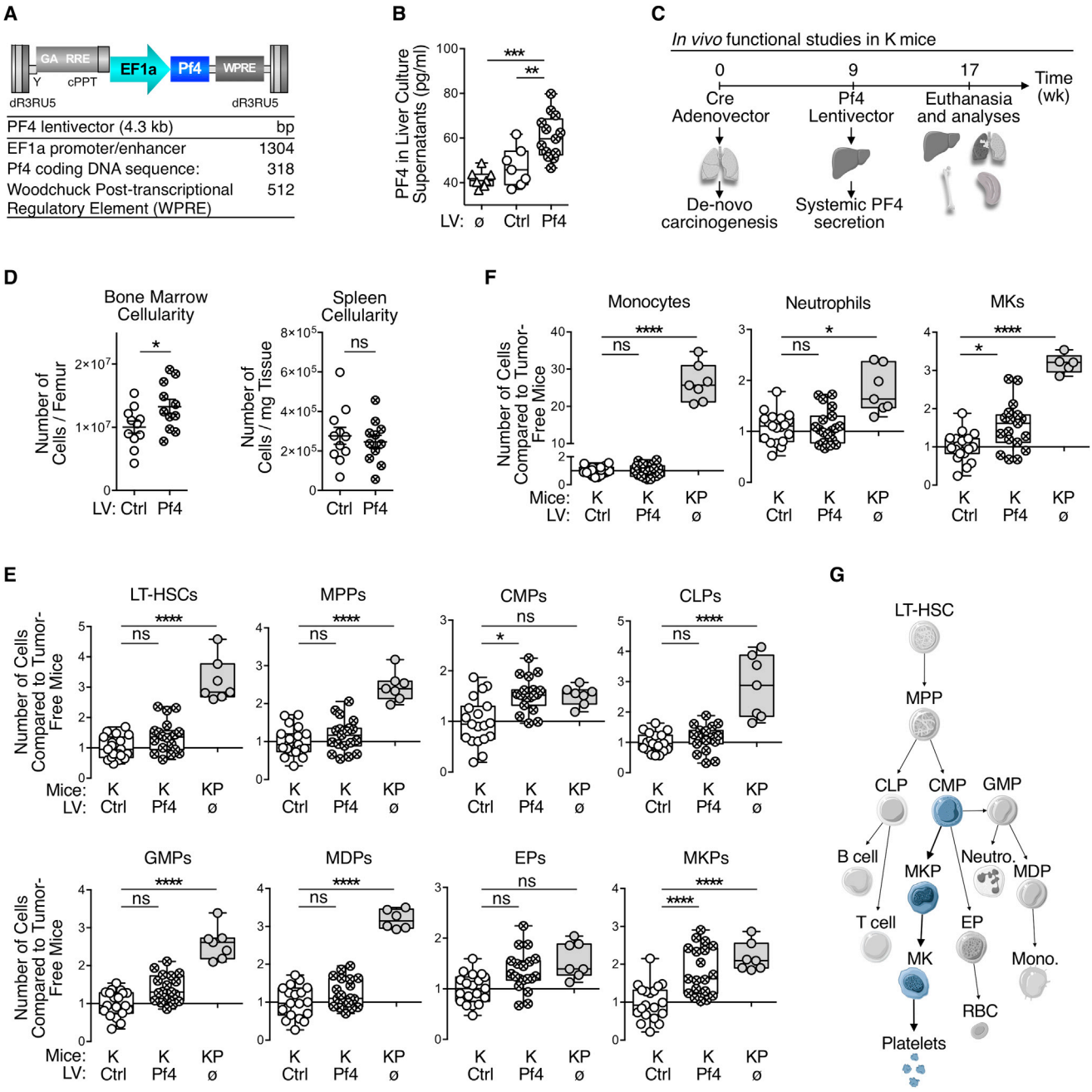

Figure 2. Systemic PF4 Production Selectively Expands the Bone Marrow Megakaryocyte Lineage

(A) Schematics of PF4-LV features. Mouse native *Pf4* coding gene is constitutively expressed under a strong promoter, without any marker gene or tag that may elicit an immune rejection of PF4-overexpressing cells.

(B) ELISA for PF4 on total liver cell culture supernatants from tumor-free (ø), Ctrl-LV-, and PF4-LV-treated K mice is shown.

(C) Illustrated experimental design. K mice were dosed intranasally with adenoviral vectors expressing Cre to activate oncogenic Kras. After 9 weeks, they received PF4-LV (or Ctrl-LV) i.v. to start systemic PF4 overexpression; at week 17, mice were euthanized and analyzed.

(D) Flow cytometry-based analysis of bone marrow (BM) and spleen total viable cells from mice treated as in (C).

(E and F) Flow cytometry-based analysis of BM hematopoietic stem/progenitor cells (E) and selected progeny (F) from mice treated as in (C). KP mice were added as controls since they natively overexpress PF4 (see Figure 1D).

(G) Cartoon depicts hematopoietic hierarchy and illustrates PF4-induced expansion of the megakaryopoietic lineage (in light blue).

Results are expressed as mean ± SEM (*$p < 0.05$, **$p < 0.01$, and ****$p < 0.0001$). Abbreviations are as follows: BM, bone marrow; CLP, common lymphoid progenitor; CMP, common myeloid progenitor; Ctrl, control; EP, erythroid progenitor; GMP, granulocyte-macrophage progenitor; K, $Kras^{G12D}$; KP, $Kras^{G12D};p53^{fl/fl}$; LT-HSCs, long-term hematopoietic stem cell; LV, lentivector; MDP, monocyte-dendritic cell progenitor; MK, megakaryocyte; MKP, megakaryocyte progenitor; MPP, multipotent progenitor; ns, not significant; RBC, red blood cell. See also Figure S2.

(Brown et al., 2006). Liver cells obtained from PF4-LV-treated K mice on week 8 post-LV injection secreted ~1.3–1.5 times more PF4 than those from either Ctrl-LV-treated K mice or tumor-free control mice (Figure 2B). Furthermore, vector copy number in liver cells remained detectable at week 8, suggesting that PF4-producing cells were not cleared by the host immune system (Figure S2B). These results indicated the possibility of modulating the expression of a candidate systemic factor and testing its impact on the host and tumor progression in mice.

Systemic PF4 Selectively Expands the Bone Marrow Megakaryocyte Lineage

To assess PF4's impact on host responses to lung cancer, we induced de novo carcinogenesis in K mice by intranasally administering Cre-expressing adenoviral vectors. Next, we instigated systemic PF4 production at week 9 by delivering PF4-LV i.v., and then we analyzed hematopoietic cells in various tissues at week 17 (Figure 2C). PF4-LV-treated K mice showed significantly increased cellularity in the bone marrow, but not in the spleen, when compared to Ctrl-LV-treated K mice (Figure 2D); this distinguishes PF4 from AGT, which instead selectively increases splenic cellularity (Cortez-Retamozo et al., 2013).

We then examined PF4's impact on bone marrow hematopoietic stem and progenitor cells and more mature immune cell lineages. We compared PF4-LV-treated and Ctrl-LV-treated K mice as mentioned above, as well as unmanipulated KP mice since their tumors naturally overexpressed *Pf4* (Figure 1D). In comparison to Ctrl-LV-treated K mice, KP mice contained more hematopoietic stem and progenitor cell populations (Figure 2E; Figure S2C), including long-term hematopoietic stem cells (LT-HSCs), multipotent progenitors (MPPs), common lymphoid progenitors (CLPs), granulocyte/macrophage progenitors (GMPs), macrophage/dendritic cell progenitors (MDPs), and megakaryocyte progenitors (MKPs). KP mice also showed more mature bone marrow immune cell lineages, including monocytes, neutrophils, and megakaryocytes (Figure 2F).

By contrast, PF4-LV treatment in K mice instigated a narrower blood lineage alteration. Among hematopoietic stem and progenitor cell populations, PF4-LV-treated K mice selectively expanded common myeloid progenitors (CMPs) and MKPs when compared to Ctrl-LV-treated K mice, while LT-HSCs, MPPs, CLPs, GMPs, and MDPs remained detectably unchanged (Figure 2E). Additionally, PF4-LV-infected K mice showed increased bone marrow megakaryocytes, but neither monocytes nor neutrophils (Figure 2F). As expected, PF4-LV-treated K mice did not have more hematopoietic stem and progenitor cells in the spleen (Figure S2D). These findings indicate that systemic PF4 overexpression specifically mediates a bone marrow megakaryopoietic response (CMPs → MKPs → megakaryocytes; Figure 2G).

PF4 Increases Platelet Accumulation in Tumor-Bearing Lungs

Based on PF4's impact on bone marrow megakaryopoiesis, we reasoned that this factor may influence the tumor microenvironment by increasing platelet accumulation. Initially, we validated a monoclonal antibody (mAb) against mouse platelet glycoprotein Ib alpha chain CD42b (Figures S3A and S3B). We then stained lung histology sections from PF4-LV- and Ctrl-LV-treated K mice as well as KP mice (Figure 3A), double-blind quantified by mCD42b signal (Figure 3B). This analysis identified increased $CD42b^+$ platelet cluster accumulation in the lungs of PF4-LV-treated mice. As expected, KP tumor-bearing lungs showed high $CD42b^+$ platelet cluster accumulation (Figures 3A and 3B).

Additional ex vivo flow cytometry-based analysis revealed that the abundance of other immune cell types remained unchanged in the lungs of PF4-LV-treated K mice as compared to their Ctrl-LV-treated counterparts (Figure 3C; Figure S3C). These data confirm that PF4 selectively amplified the megakaryocyte lineage in the bone marrow without affecting the lymphoid cell and phagocyte lineages. The selective change in platelet accumulation at the tumor site indicates PF4 drives this phenotype directly (as opposed to PF4 affecting other cells that would then recruit platelets to the tumor stroma).

To test whether the results detailed above had clinical correlates, we assessed platelet accumulation in lung adenocarcinoma patients. We used an anti-human CD42b mAb that, we confirmed, labels $CD45^-$ platelets and does not cross-react with other $CD45^+$ white blood cells (Figure S3D). We then assessed tumor infiltration by platelets in 29 tumor biopsy sections from non-small-cell lung cancer (NSCLC) patients genotyped for *KRAS* and *TP53* mutations. *KRAS*/*TP53*-mutated tumors showed increased platelet infiltration when compared to *KRAS*- and *TP53*-mutated tumors and tumor-free tissue (Figures 3D and 3E; Figure S3E). Although the number of patients carrying both mutations was limited, these findings indicate that platelets efficiently accumulate in at least a fraction of human lung tumors and that the K and KP mouse models are relevant for studying tumors that share features with their human counterparts.

Platelets and Circulating PF4 Promote Kras-Driven Lung Adenocarcinogenesis

Treatment of KP tumor-bearing mice with clopidogrel, an inhibitor of platelet aggregation and activation (Quinn and Fitzgerald, 1999), reduced cancer growth, as characterized by decreased lung weight (Figure 4A) and lung tumor burden (Figures 4B and 4C). Clopidogrel-treated mice, but not the PBS-treated controls, also maintained their overall body weight (Figure S4A) during the course of the experiment. These results indicate that platelets enhance KP tumor growth.

Conversely, we asked whether systemically increased PF4 production accelerates de novo lung tumor progression in K mice. Indeed, we found increased lung weights in PF4-LV-treated K mice as compared to their Ctrl-LV-treated counterparts (Figure 4D). We also generated whole-lung histological sections to evaluate whether PF4-LV-treated K mice's heavier lungs were due to higher tumor burden (Figure 4E). Quantified tumor area in these sections confirmed elevated tumor burden in PF4-LV-treated compared to control mice (Figure 4F). We also noted more tumor foci in PF4-LV mice than in their Ctrl-LV counterparts (Figure 4G). Together, these results provide in vivo evidence that increased systemic PF4 levels accelerate K tumor progression. PF4 did not accelerate K tumor growth in isolation in vitro (Figure S4B), further indicating that increased PF4 production fosters tumor growth by acting on host cell components.

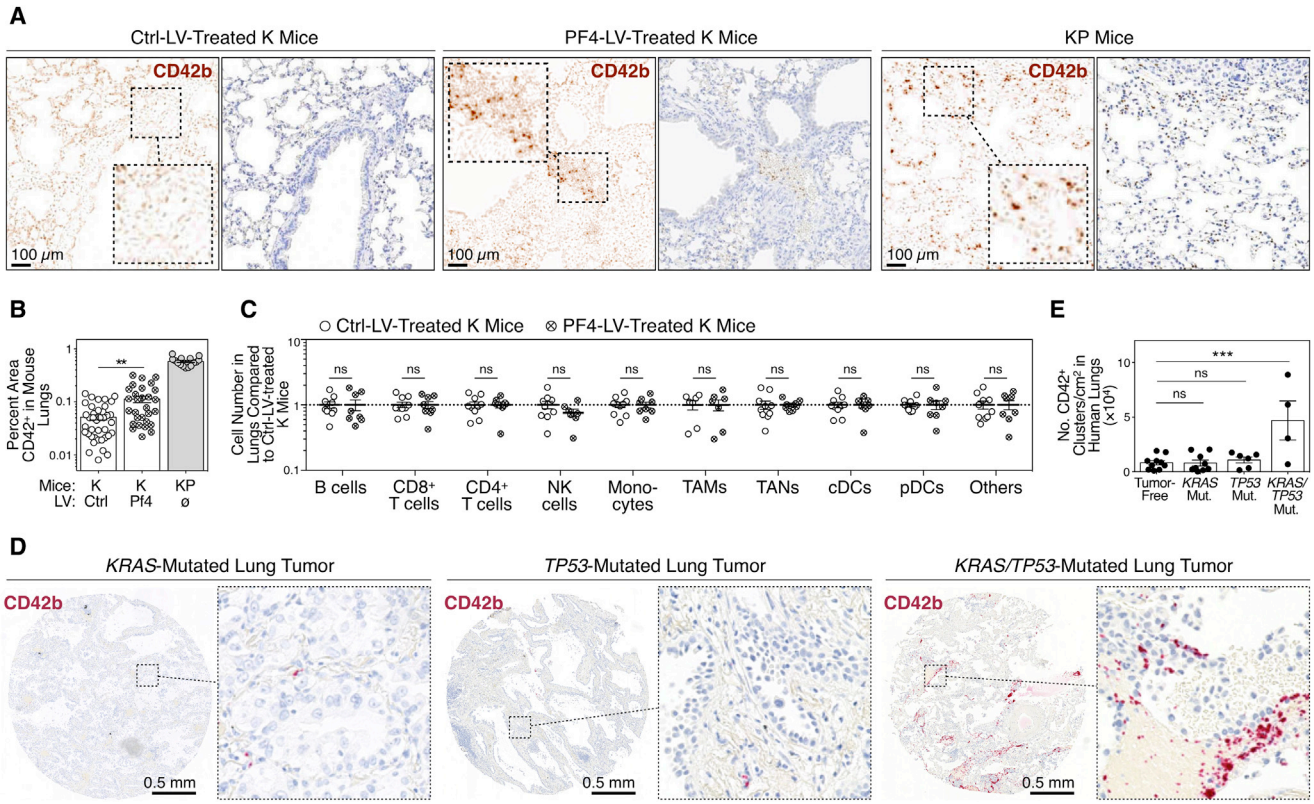

Figure 3. Systemic PF4 Production Amplifies Platelet Accumulation at the Tumor Site

(A) Immunohistochemistry staining for mCD42b (dark brown) on lung sections from K mice treated with either Ctrl- or PF4-LV and from KP mice. Left panels show mCD42b signal (split brown channels), whereas right panels show original DAB staining (brown) with hematoxylin counterstain (blue). Scale bars represent 100 μm.

(B) Quantification of percentage mCD42b+ areas per field of views, based on immunohistochemistry staining in (A), is shown.

(C) Flow cytometry-based quantification of various immune cell types in the lungs of K mice treated with either Ctrl- or PF4-LV is shown.

(D) Immunohistochemistry staining for hCD42b (red) on lung cancer patient tissue microarrays. Representative biopsies of *KRAS*-mutated (left), *TP53*-mutated (center), and both *KRAS*- and *TP53*-mutated tumors (right) are shown. Scale bars represent 0.5 mm.

(E) Quantification of hCD42b+ clusters per square centimeter, based on immunohistochemistry staining in (D), is shown.

Results are expressed as mean ± SEM (**p < 0.01 and ***p < 0.001). Abbreviations are as follows: cDC, classical dendritic cell; ctrl, control; K, $Kras^{G12D}$; KP, $Kras^{G12D}$;$p53^{fl/fl}$; LV, lentivector; mono., monocyte; mut., mutant; NK, natural killer; ns, not significant; pDC, plasmacytoid dendritic cell; TAM, tumor-associated macrophage; TAN, tumor-associated neutrophil. See also Figure S3.

DISCUSSION

By cross-analyzing selected datasets from human and mouse lung adenocarcinomas, we identified candidate factors that may act as endocrine signals in tumor-host communication. Furthermore, by manipulating systemic PF4 production, we validated this factor as a key constituent that alters discrete components of the tumor-associated host response and accelerates adenocarcinogenesis. Previous studies indicated that PF4 in steady state suppresses megakaryopoiesis (Lambert et al., 2007; Oda et al., 2003) and induces hematopoietic stem cell quiescence (Bruns et al., 2014; Zhao et al., 2014) but can promote hematopoiesis and megakaryopoiesis under stress conditions, such as radiotherapy or chemotherapy (Aidoudi et al., 1996; Bruns et al., 2014; Caen et al., 1999). Here, in the context of cancer, we found a causal link between increased endogenous PF4 levels and (1) expanded megakaryopoiesis, (2) platelet accumulation in cancer-developing lungs, and (3) accelerated tumor growth. That PF4 triggers these phenotypes during carcinogenesis accords with our understanding that cancer puts chronic stress on the hematopoietic system (Shalapour and Karin, 2015).

PF4-induced platelet accumulation in tumors is important because platelets can modulate tumor cells and the tumor microenvironment to accelerate cancer outgrowth. For example, platelets can promote tumor angiogenesis (Ho-Tin-Noé et al., 2008; Kuznetsov et al., 2012; Qi et al., 2015; Gebremeskel et al., 2015; Mezouar et al., 2015), prevent tumor cell recognition by natural killer cells (Nieswandt et al., 1999; Palumbo et al., 2005; Placke et al., 2012), and foster metastasis by recruiting myeloid cells into metastatic niches (Gay and Felding-Habermann, 2011; Labelle et al., 2014). Here we provide evidence for a direct role of PF4 in platelet accumulation in lung tumors, both in mouse models and patients.

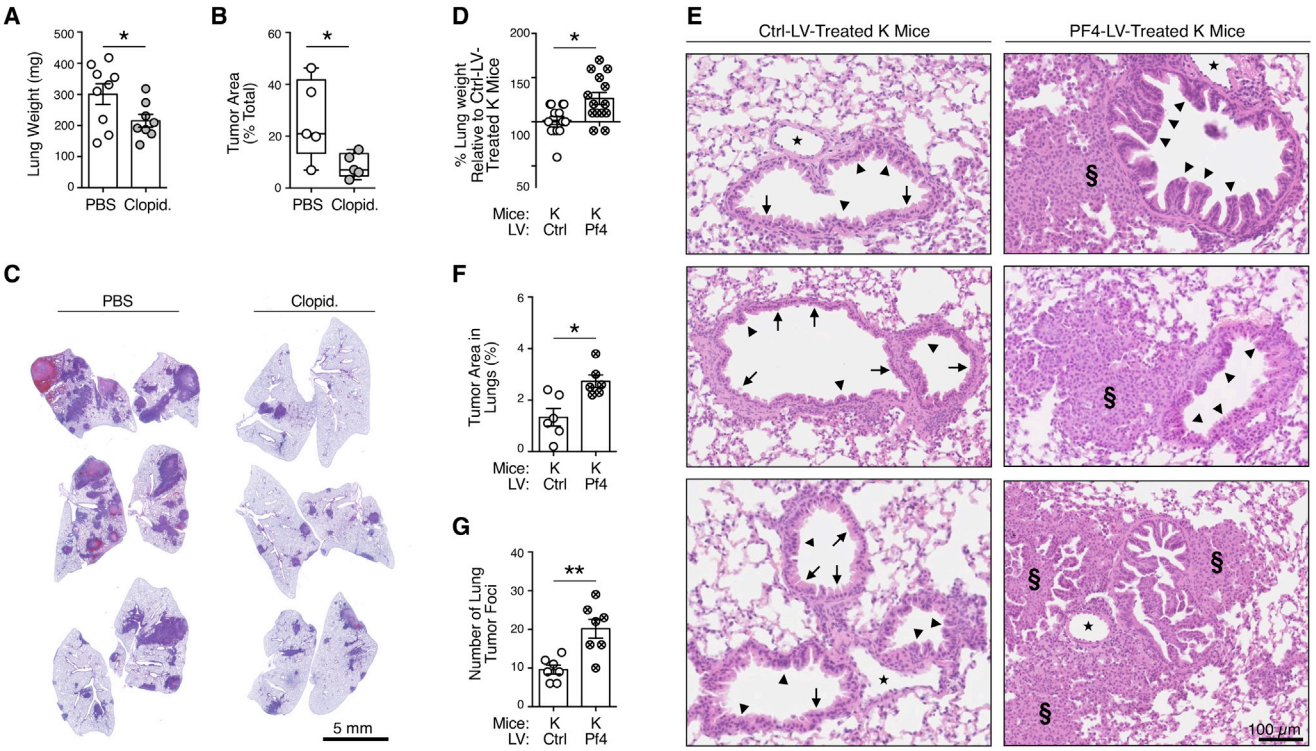

Figure 4. Platelets and Systemic PF4 Production Promote Cancer Progression

(A) Lung weight of PBS-treated and clopidogrel-treated tumor-bearing mice 5 weeks after KP1.9 lung tumor cell injection is shown.

(B) Histochemistry-based quantification of total tumor areas (as percentage of total lung section areas) in PBS- and clopidogrel-treated KP1.9 tumor bearing mice is shown.

(C) Representative H&E images show lung sections from the same mice as in (B).

(D) Lung weight of Ctrl-LV- and PF4-LV-treated K mice 17 weeks after tumor initiation. Data are shown as the percentage of Ctrl-LV lung weight.

(E) Representative H&E images show lung sections from the same mice as in (A). Asterisks, blood vessels; arrows, normal epithelia; triangles, hyperplasia; symbols, adenoma. Scale bars represent 100 μm.

(F and G) Histochemistry-based quantifications of total tumor areas (as percentage of total lung section areas) (E) and lung tumor foci (F) in Ctrl-LV- and PF4-LV-treated K mice are shown.

Results are expressed as mean ± SEM (*$p < 0.05$ and **$p < 0.01$). Abbreviations are as follows: Clopid, clopidogrel; Ctrl, control; K, $Kras^{G12D}$; LV, lentivector. See also Figure S4.

PF4 analogs or fragments can be anti-angiogenic and by extension exert antitumor activities (Giussani et al., 2003; Maione et al., 1991; Tanaka et al., 1997). However, increased circulating native PF4 levels are associated with human lung cancer (Taguchi et al., 2011; Engels et al., 2015). Importantly, in this study we used a *Pf4* expression cassette that produced native PF4 in vivo. With this approach, we not only confirmed a positive association between native *Pf4* overexpression and faster tumor progression but also identified PF4 as a causal factor driving this phenotype.

Systemically increased PF4 production during de novo carcinogenesis selectively amplified medullary megakaryopoiesis and platelet accumulation at the tumor site. These findings indicate a specific control that is operated by tumors on the host and that extends beyond the local tumor microenvironment. KP tumors overexpress several factors, including *Pf4* (as per this study) and *Agt* (Cortez-Retamozo et al., 2013), yet PF4's effects on medullary megakaryopoiesis were distinct from those of AGT (the Angiotensin II precursor) on extramedullary monocytopoiesis. Consequently, we propose that lung tumors can remotely control distinct hematopoietic cells by producing different endocrine factors. These factors (PF4, Angiotensin II, and likely others) shape the tumor microenvironment, consequently alter tumor progression, and may thus be promising molecular targets for anticancer therapy.

EXPERIMENTAL PROCEDURES

Mice

$Kras^{LSL-G12D/+}$;$p53^{fl/fl}$ (referred to as KP) and $Kras^{LSL-G12D/+}$ (referred to as K) mice in a 129/j background were used as conditional mouse models of lung adenocarcinoma, as described previously (Cortez-Retamozo et al., 2012). All animal experiments were approved by the Massachusetts General Hospital Subcommittee on Research Animal Care. Methods to induce lung adenocarcinoma in these mice are described in the Supplemental Experimental Procedures.

Human Tumor Samples

Sections from paraffin-embedded lung resection biopsies (n = 29) from NSCLC patients with known *KRAS* and *TP53* gene mutation status were

obtained from the Department of Pathology at Massachusetts General Hospital. CD42b immunohistochemistry was performed and evaluated blindly as described in the Supplemental Experimental Procedures.

PF4 LVs

Concentrated VSV.G-pseudotyped, third-generation LV stocks were produced and titered as described previously (De Palma and Naldini, 2002). LV copy per genome (CpG) of samples was calculated using genomic DNA standard curve with known CpG. The CpG of genomic DNA standard curves and samples was determined using custom TaqMan assays specific for LVs (Applied Biosystems). LVs were injected i.v. 2×10^4 ng p24/mouse in 50–200 μl, depending on the infectivity.

Bioinformatics and Statistics

In silico analyses were performed in R. The initial list of murine candidates used to probe the lung cancer patient microarray dataset was sequentially transformed from a list of murine proteins into the following: (1) their human orthologs, (2) their gene symbols, and (3) the corresponding microarray probe identifications. The list of microarray probes was matched with human datasets for survival analysis, which used the log-rank test. GraphPad Prism 6 was used for all statistical analyses. Statistical tests for multivariate analyses were performed using two-way ANOVA followed by Holm-Sidak multiple comparison test. The p values were considered significant at <0.05.

Gene and Protein Nomenclature

Capitalization of gene and protein symbols is styled according to species (human gene symbol, *PF4*; protein symbol, PF4; mouse gene symbol, Pf4; protein symbol, PF4).

SUPPLEMENTAL INFORMATION

Supplemental Information includes Supplemental Experimental Procedures and four figures and can be found with this article online at http://dx.doi.org/10.1016/j.celrep.2016.10.031.

AUTHOR CONTRIBUTIONS

F.P. and M.J.P. conceived the research plan and wrote the manuscript. F.P., S.R., C.G., C.P., and C. Engblom performed research and analyzed data. A.P.N., C. Evavold, and M.M.-K. performed research. E.N. computer coded and analyzed data. R.O.H., R.W., and M.J.P. analyzed data and supervised the work.

ACKNOWLEDGMENTS

This work was supported in part by the Samana Cay MGH Research Scholar Fund to M.J.P.; NIH grants R21-CA190344, P50-CA86355, and R01-AI084880 to M.J.P., U54-CA126515 to R.W., U54-CA163109 to R.O.H., and F31-CA196035 to C.G.; European Molecular Biology Organization (EMBO) long-term fellowship (ALTF 1535-2011) and Massachusetts General Hospital Executive Committee On Research (ECOR) Funds for Medical Discovery Fellowship to F.P.; Deutsche Forschungsgemeinschaft PF809/1-1 to C.P. and RI2408/1-1 to S.R.; Metastasis/Cancer Research Postdoc fellowship from MIT Ludwig Center for Molecular Oncology Research to S.R.; Boehringer Ingelheim Funds to C. Engblom; and the Howard Hughes Medical Institute to R.O.H. The authors thank the members of the Hope Babette Tang Histology Facility at the Koch Institute Swanson Biotechnology Center, Yoshiko Iwamoto of the Center for System Biology for technical support, and Dr. Wouter Meuleman for help with R coding.

Received: March 8, 2016
Revised: September 2, 2016
Accepted: October 11, 2016
Published: November 8, 2016

REFERENCES

Aidoudi, S., Guigon, M., Lebeurier, I., Caen, J.P., and Han, Z.C. (1996). In vivo effect of platelet factor 4 (PF4) and tetrapeptide AcSDKP on haemopoiesis of mice treated with 5-fluorouracil. Br. J. Haematol. *94*, 443–448.

Brown, B.D., Venneri, M.A., Zingale, A., Sergi Sergi, L., and Naldini, L. (2006). Endogenous microRNA regulation suppresses transgene expression in hematopoietic lineages and enables stable gene transfer. Nat. Med. *12*, 585–591.

Bruns, I., Lucas, D., Pinho, S., Ahmed, J., Lambert, M.P., Kunisaki, Y., Scheiermann, C., Schiff, L., Poncz, M., Bergman, A., and Frenette, P.S. (2014). Megakaryocytes regulate hematopoietic stem cell quiescence through CXCL4 secretion. Nat. Med. *20*, 1315–1320.

Caen, J.P., Han, Z.C., Bellucci, S., and Alemany, M. (1999). Regulation of megakaryocytopoiesis. Haemostasis *29*, 27–40.

Casbon, A.J., Reynaud, D., Park, C., Khuc, E., Gan, D.D., Schepers, K., Passegué, E., and Werb, Z. (2015). Invasive breast cancer reprograms early myeloid differentiation in the bone marrow to generate immunosuppressive neutrophils. Proc. Natl. Acad. Sci. USA *112*, E566–E575.

Cortez-Retamozo, V., Etzrodt, M., Newton, A., Rauch, P.J., Chudnovskiy, A., Berger, C., Ryan, R.J., Iwamoto, Y., Marinelli, B., Gorbatov, R., et al. (2012). Origins of tumor-associated macrophages and neutrophils. Proc. Natl. Acad. Sci. USA *109*, 2491–2496.

Cortez-Retamozo, V., Etzrodt, M., Newton, A., Ryan, R., Pucci, F., Sio, S.W., Kuswanto, W., Rauch, P.J., Chudnovskiy, A., Iwamoto, Y., et al. (2013). Angiotensin II drives the production of tumor-promoting macrophages. Immunity *38*, 296–308.

De Palma, M., and Naldini, L. (2002). Transduction of a gene expression cassette using advanced generation lentiviral vectors. Methods Enzymol. *346*, 514–529.

DuPage, M., Dooley, A.L., and Jacks, T. (2009). Conditional mouse lung cancer models using adenoviral or lentiviral delivery of Cre recombinase. Nat. Protoc. *4*, 1064–1072.

Engblom, C., Pfirschke, C., and Pittet, M.J. (2016). The role of myeloid cells in cancer therapies. Nat. Rev. Cancer *16*, 447–462.

Engels, E.A., Jennings, L., Kemp, T.J., Chaturvedi, A.K., Pinto, L.A., Pfeiffer, R.M., Trotter, J.F., Acker, M., Onaca, N., and Klintmalm, G.B. (2015). Circulating TGF-β1 and VEGF and risk of cancer among liver transplant recipients. Cancer Med. *4*, 1252–1257.

Gay, L.J., and Felding-Habermann, B. (2011). Contribution of platelets to tumour metastasis. Nat. Rev. Cancer *11*, 123–134.

Gebremeskel, S., LeVatte, T., Liwski, R.S., Johnston, B., and Bezuhly, M. (2015). The reversible P2Y12 inhibitor ticagrelor inhibits metastasis and improves survival in mouse models of cancer. Int. J. Cancer *136*, 234–240.

Giussani, C., Carrabba, G., Pluderi, M., Lucini, V., Pannacci, M., Caronzolo, D., Costa, F., Minotti, M., Tomei, G., Villani, R., et al. (2003). Local intracerebral delivery of endogenous inhibitors by osmotic minipumps effectively suppresses glioma growth in vivo. Cancer Res. *63*, 2499–2505.

Hanahan, D., and Coussens, L.M. (2012). Accessories to the crime: functions of cells recruited to the tumor microenvironment. Cancer Cell *21*, 309–322.

Ho-Tin-Noé, B., Goerge, T., Cifuni, S.M., Duerschmied, D., and Wagner, D.D. (2008). Platelet granule secretion continuously prevents intratumor hemorrhage. Cancer Res. *68*, 6851–6858.

Kuznetsov, H.S., Marsh, T., Markens, B.A., Castaño, Z., Greene-Colozzi, A., Hay, S.A., Brown, V.E., Richardson, A.L., Signoretti, S., Battinelli, E.M., and McAllister, S.S. (2012). Identification of luminal breast cancers that establish a tumor-supportive macroenvironment defined by proangiogenic platelets and bone marrow-derived cells. Cancer Discov. *2*, 1150–1165.

Labelle, M., Begum, S., and Hynes, R.O. (2014). Platelets guide the formation of early metastatic niches. Proc. Natl. Acad. Sci. USA *111*, E3053–E3061.

Lambert, M.P., Rauova, L., Bailey, M., Sola-Visner, M.C., Kowalska, M.A., and Poncz, M. (2007). Platelet factor 4 is a negative autocrine in vivo regulator of megakaryopoiesis: clinical and therapeutic implications. Blood *110*, 1153–1160.

Maione, T.E., Gray, G.S., Hunt, A.J., and Sharpe, R.J. (1991). Inhibition of tumor growth in mice by an analogue of platelet factor 4 that lacks affinity for heparin and retains potent angiostatic activity. Cancer Res. *51*, 2077–2083.

McAllister, S.S., and Weinberg, R.A. (2014). The tumour-induced systemic environment as a critical regulator of cancer progression and metastasis. Nat. Cell Biol. *16*, 717–727.

McAllister, S.S., Gifford, A.M., Greiner, A.L., Kelleher, S.P., Saelzler, M.P., Ince, T.A., Reinhardt, F., Harris, L.N., Hylander, B.L., Repasky, E.A., and Weinberg, R.A. (2008). Systemic endocrine instigation of indolent tumor growth requires osteopontin. Cell *133*, 994–1005.

Mezouar, S., Darbousset, R., Dignat-George, F., Panicot-Dubois, L., and Dubois, C. (2015). Inhibition of platelet activation prevents the P-selectin and integrin-dependent accumulation of cancer cell microparticles and reduces tumor growth and metastasis in vivo. Int. J. Cancer *136*, 462–475.

Nguyen, D.X., Chiang, A.C., Zhang, X.H., Kim, J.Y., Kris, M.G., Ladanyi, M., Gerald, W.L., and Massagué, J. (2009). WNT/TCF signaling through LEF1 and HOXB9 mediates lung adenocarcinoma metastasis. Cell *138*, 51–62.

Nieswandt, B., Hafner, M., Echtenacher, B., and Männel, D.N. (1999). Lysis of tumor cells by natural killer cells in mice is impeded by platelets. Cancer Res. *59*, 1295–1300.

Oda, M., Kurasawa, Y., Todokoro, K., and Nagata, Y. (2003). Thrombopoietin-induced CXC chemokines, NAP-2 and PF4, suppress polyploidization and proplatelet formation during megakaryocyte maturation. Genes Cells *8*, 9–15.

Palumbo, J.S., Talmage, K.E., Massari, J.V., La Jeunesse, C.M., Flick, M.J., Kombrinck, K.W., Jirousková, M., and Degen, J.L. (2005). Platelets and fibrin(ogen) increase metastatic potential by impeding natural killer cell-mediated elimination of tumor cells. Blood *105*, 178–185.

Pittet, M.J., Nahrendorf, M., and Swirski, F.K. (2014). The journey from stem cell to macrophage. Ann. N Y Acad. Sci. *1319*, 1–18.

Placke, T., Örgel, M., Schaller, M., Jung, G., Rammensee, H.G., Kopp, H.G., and Salih, H.R. (2012). Platelet-derived MHC class I confers a pseudonormal phenotype to cancer cells that subverts the antitumor reactivity of natural killer immune cells. Cancer Res. *72*, 440–448.

Poruk, K.E., Firpo, M.A., Huerter, L.M., Scaife, C.L., Emerson, L.L., Boucher, K.M., Jones, K.A., and Mulvihill, S.J. (2010). Serum platelet factor 4 is an independent predictor of survival and venous thromboembolism in patients with pancreatic adenocarcinoma. Cancer Epidemiol. Biomarkers Prev. *19*, 2605–2610.

Qi, C., Li, B., Guo, S., Wei, B., Shao, C., Li, J., Yang, Y., Zhang, Q., Li, J., He, X., et al. (2015). P-selectin-mediated adhesion between platelets and tumor cells promotes intestinal tumorigenesis in Apc(Min/+) mice. Int. J. Biol. Sci. *11*, 679–687.

Quinn, M.J., and Fitzgerald, D.J. (1999). Ticlopidine and clopidogrel. Circulation *100*, 1667–1672.

Shalapour, S., and Karin, M. (2015). Immunity, inflammation, and cancer: an eternal fight between good and evil. J. Clin. Invest. *125*, 3347–3355.

Shedden, K., Taylor, J.M., Enkemann, S.A., Tsao, M.S., Yeatman, T.J., Gerald, W.L., Eschrich, S., Jurisica, I., Giordano, T.J., Misek, D.E., et al.; Director's Challenge Consortium for the Molecular Classification of Lung Adenocarcinoma (2008). Gene expression-based survival prediction in lung adenocarcinoma: a multi-site, blinded validation study. Nat. Med. *14*, 822–827.

Taguchi, A., Politi, K., Pitteri, S.J., Lockwood, W.W., Faça, V.M., Kelly-Spratt, K., Wong, C.H., Zhang, Q., Chin, A., Park, K.S., et al. (2011). Lung cancer signatures in plasma based on proteome profiling of mouse tumor models. Cancer Cell *20*, 289–299.

Tanaka, T., Manome, Y., Wen, P., Kufe, D.W., and Fine, H.A. (1997). Viral vector-mediated transduction of a modified platelet factor 4 cDNA inhibits angiogenesis and tumor growth. Nat. Med. *3*, 437–442.

Torre, L.A., Siegel, R.L., and Jemal, A. (2016). Lung cancer statistics. Adv. Exp. Med. Biol. *893*, 1–19.

Zhao, M., Perry, J.M., Marshall, H., Venkatraman, A., Qian, P., He, X.C., Ahamed, J., and Li, L. (2014). Megakaryocytes maintain homeostatic quiescence and promote post-injury regeneration of hematopoietic stem cells. Nat. Med. *20*, 1321–1326.

Cell Reports, Volume *17*

Supplemental Information

PF4 Promotes Platelet Production and Lung Cancer Growth

Ferdinando Pucci, Steffen Rickelt, Andita P. Newton, Christopher Garris, Ernesto Nunes, Charles Evavold, Christina Pfirschke, Camilla Engblom, Mari Mino-Kenudson, Richard O. Hynes, Ralph Weissleder, and Mikael J. Pittet

Supplemental Information

Inventory of Supplemental Items

- Figure S1-S4
- Supplemental Experimental Procedures
- Supplemental References

Supplemental Figures and Legends

A

Over-Abundant Proteins in Plasma	
Protein	Fold change
Adam10	1.5
Adamts2	1.3
Agt	1.3
Ak1	1.5
Angptl3	1.8
Apcs	2.1
Coro1a	1.3
Eif2ak3	9.0
F7	1.3
Fgfr2	Cancer only
Hamp2	3.1
Igfbp4	1.4
Igsf4a	1.5
Ltbp2	1.4
Lyzs	1.8
Man2b2	1.5
Morc3	10.0
Ncan	1.5
Npc2	3.5
Nup188	Cancer only
Pf4	1.6
Pglyrp1	1.4
Ppbp	1.7
Ppia	1.3
Prtg	10.0
Rarres2	2.5
Sftpb	3.4
Slit2	Cancer only
Son	10.0
Tfpi2	Cancer only
Tspan5	10.0
Vnn3	1.3
Wfdc2	2.3

Under-Abundant Proteins in Plasma	
Protein	Fold change
Arg1	0.1
C1r	0.8
C6	0.2
C8a	0.2
C8b	0.3
C9	0.3
Camta2	0.1
Cand2	0.1
Egfr	0.4
Hamp1	0.3
Hp	0.4
Mug1	0.4
Mup1	0.2
Mup2	0.3
Notch1	0.5
Pam	0.2
Pear1	0.1
Pon1	0.7
Prg4	0.6
Proz	0.8
Rgn	0.2
Sepp1	0.7
Serpina3k	0.6
Smarcc2	0.1
Tfpi	0.5
Thumpd1	0.1
Wdr62	0.4

B

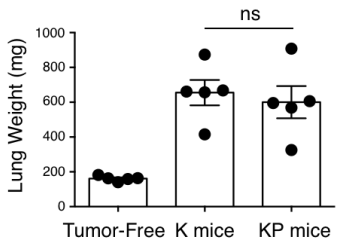

C

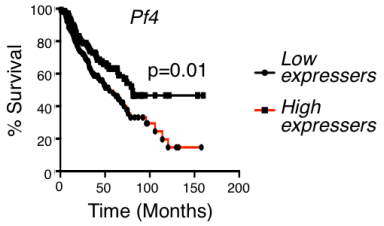

D

Demographic and clinical characteristics of two cohorts of lung cancer patients

Variable	*PF4^{hi}* (n=133)	*PF4^{lo}* (n=133)	P Value
Median age (range) — yr	65.1 (36-87)	64.4 (33-89)	0.563
Male sex — %	53	45	0.270
Smoking history — Cases			0.636
Currently smoking	9	11	
Never smoked	69	70	
Smoked in the past	16	10	
Unknown	39	42	
Histologic grade — Cases			0.890
Well differentiated	9	11	
Moderate differentiation	28	31	
Poorly differentiated	32	28	
Unknown	64	63	
Stage — Cases			0.298
IA	31	45	
IB	51	52	
IIA	4	5	
IIB	3	2	
IIIA/B	26	16	
IIIC/IV	18	13	
Adjuvant chemotherapy — Cases			0.325
No	47	47	
Yes	72	64	
Unknown	14	22	
Adjuvant radiation therapy — Cases			0.586
No	50	55	
Yes	72	64	
Unknown	11	14	
EGFR mutation — Cases			0.544
Unknown	108	108	
Ex19	4	1	
Ex21	2	0	
L858R	0	2	
Negative	19	22	
KRAS mutation — Cases			0.949
Unknown	108	108	
G12A	0	1	
G12C	2	2	
G12D	3	0	
G12V	1	3	
G13C	0	1	
Negative	19	18	

Figure S1. Related to Figure 1. Identification of candidate long-range factors associated with altered survival in lung adenocarcinoma.

(**A**) Plasma proteins over- or under-abundant in lung adenocarcinoma murine models as previously published (Taguchi et al., 2011).

(**B**) Lung weight as proxy for tumor burden in mice used for gene expression analysis in Figure 1D-E.

(**C**) Kaplan-Meier survival curves for patients with highest (top 20%, n = 133) and lowest (bottom 20%, n = 133) mRNA expression levels for *Pf4*. Data are from 4 additional datasets (Nguyen et al., 2009).

(**D**) Contingency table comparing clinical covariates corresponding to the pooled top 20% highest *PF4* expressers (*PF4^{HI}*) and bottom 20% lowest *PF4* expressers (*PF4^{LO}*). Data were associated to the microarray datasets used for survival analysis presented in Fig 1B-C and S1B-C. Median age is shown in years (yr) and all other variables are presented as number of patients for each cohort (*PF4^{HI}* or *PF4^{LO}*). Unpaired 2-tailed Student's t test was performed to compare age groups. Fisher's exact test or chi-squared test were performed to compare frequency distributions. *p < 0.05. Abbreviations are as follows: K, *Kras^{G12D}*; KP, *Kras^{G12D};p53$^{fl/fl}$*; ns, not significant.

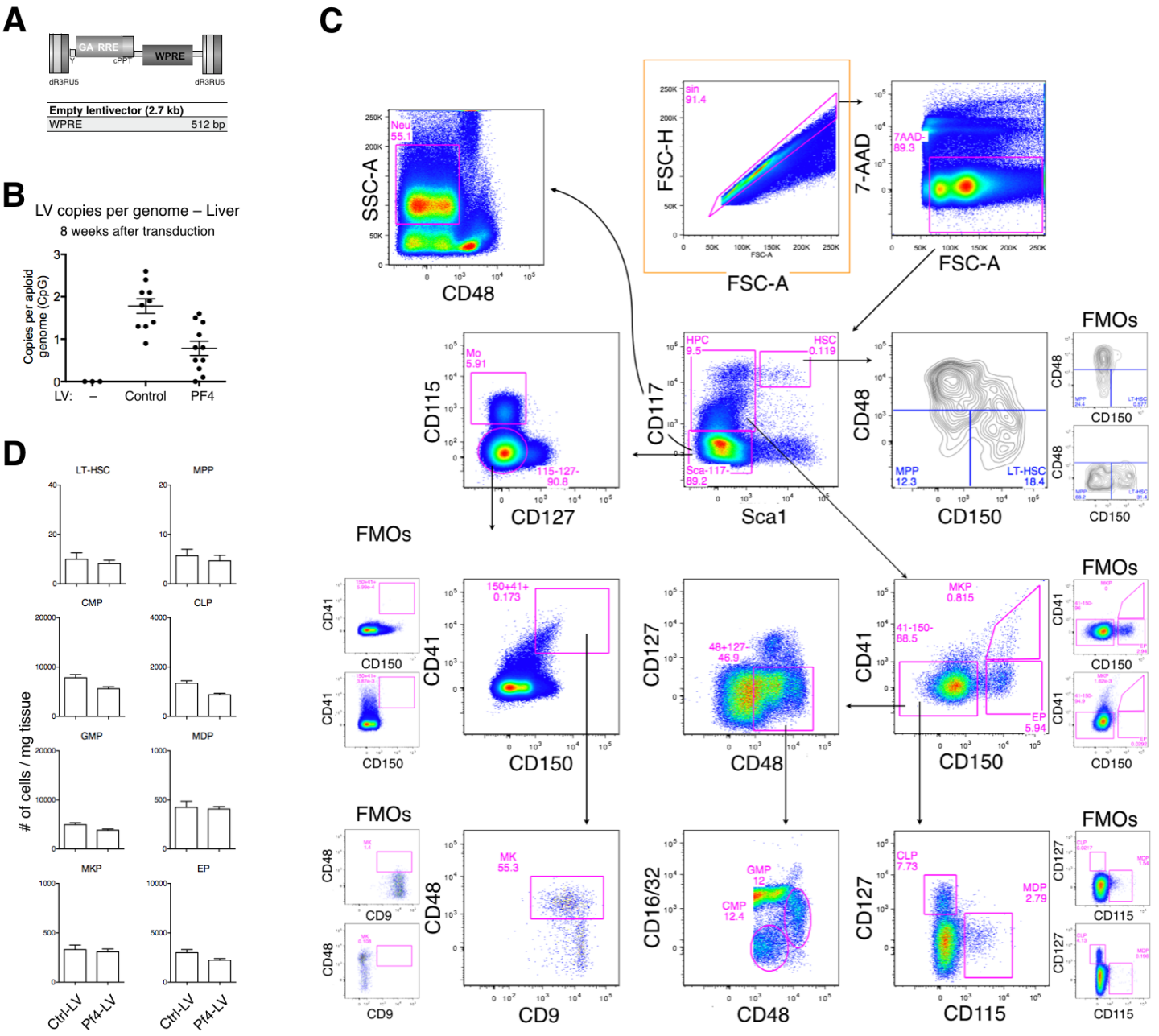

Figure S2. Related to Figure 2. Study of BM and spleen hemopoiesis after systemic PF4 over-expression in K mice

(**A**) Features of Ctrl-LV. Ctrl-LV is "empty" since it does not contains an expression cassette.

(**B**) Analysis of LV copy number in liver from mice treated with the indicated LV eight weeks earlier. Each dot corresponds to one mouse.

(**C**) Gating strategy used to quantify bone marrow and spleen cell subsets in Fig 2E-F. Orange outline define initial ungated plot. Sequential gating on regions is indicated by arrows. FMO (fluorescence minus one) controls are on the side of relevant plots.

(**D**) Flow cytometry-based analysis of splenic hemopoietic stem/progenitor cells from mice treated as in Fig. 2C.

Abbreviations are as follows: CLP, common lymphoid progenitors; CMP, common myeloid progenitors; Ctrl-LV, Control lentivector; EP, erythroid progenitors; FMO, fluorescence minus one; GMP, granulocyte-macrophage progenitors; LT-HSC, long-term hemopoietic stem cells; HPC, hemopoietic progenitor cells; MDP, monocyte-dendritic cell progenitors; MK, megakaryocyte; MKP, megakaryocyte progenitors; Mo, monocytes; MPP, multi-potent progenitors; Neu, neutrophils; Pf4-LV, Pf4 lentivector; sin, singlets; WPRE, Woodchuck hepatitis virus Post-transcriptional Regulatory Element.

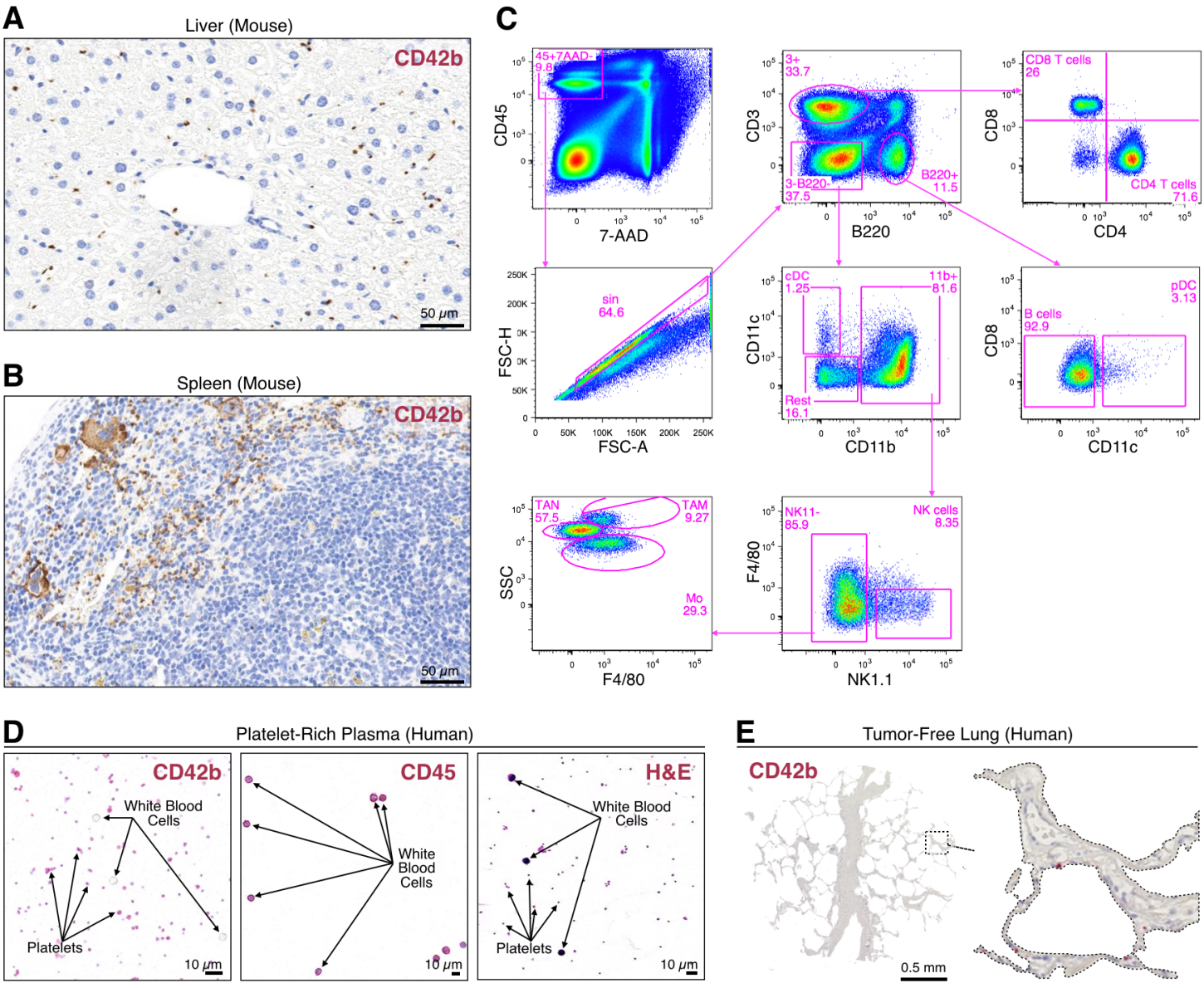

Figure S3. Related to Figure 3. Controls for staining platelets in murine and patient lung-tumor sections and for labeling murine tumor-infiltrating immune-cell subsets in flow-cytometry experiments.

(**A-B**) Immunohistochemistry staining for mCD42b (dark brown) on sections of liver (**A**) and spleen (**B**) from control mice. Scale bars represent 50 μm. Large megakaryocytes are visible in the subcapsular region of the spleen.

(**C**) Gating strategy used to quantify lung cell subsets in Fig 3C. Top left panel represent initial ungated plot. Sequential gating on regions is indicated by arrows.

(**D**) Immunohistochemistry staining for hCD42b (red, leftmost panel), hCD45 (red, middle panel) and hematoxylin and eosin (rightmost panel) on human platelet-rich plasma preparations.

(**E**) Immunohistochemistry staining for hCD42b (red) on lung cancer patient tissue microarrays. A representative example of non-involved, tumor-free tissue is shown.

Abbreviations are as follows: cDC, common dendritic cells; pDC, plasmacytoid dendritic cells; Mo, monocytes; NK, natural killer; sin, singlets; TAM, tumor-associated macrophages; TAN, tumor-associated neutrophils.

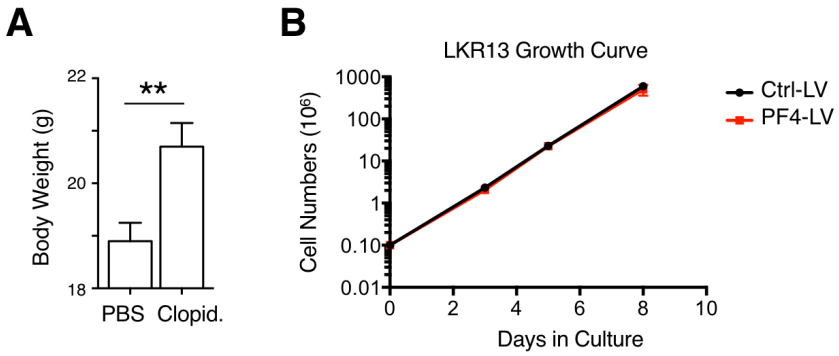

Figure S4. Related to Figure 4. Platelet-targeting agents influence cancer growth in a non-tumor cell autonomous manner.
(**A**) Body weight of PBS-treated and Clopidogrel-treated tumor-bearing mice 5 weeks after KP1.9 lung tumor cell injection (n=8-9).
(**B**) Growth curves of Kras lung-tumor cell line LKR13 transduced with either Ctrl- or PF4-LV.

Supplemental Experimental Procedures

Mice

Kras$^{LSL-G12D/+}$;*p53*$^{fl/fl}$ (referred to as KP) and *Kras*$^{LSL-G12D/+}$ (referred to as K) mice in a 129/j background were used as conditional mouse models of lung adenocarcinoma as described previously (Cortez-Retamozo et al., 2012). To induce lung adenocarcinoma, KP and K mice were infected with an adenovirus expressing Cre recombinase (AdCre) by intranasal instillation, as described previously (DuPage et al., 2009). AdCre was purchased from the University of Iowa Gene Transfer Vector Core. Control 129 mice were bought from The Jackson Laboratory. All animal experiments were approved by the Massachusetts General Hospital Subcommittee on Research Animal Care.

PF4 lentiviral vectors

Concentrated VSV.G-pseudotyped, third-generation LV stocks were produced and titered as described previously (De Palma and Naldini, 2002). Lentiviral vector copy per genome (CpG) was calculated by titering the concentrated LV on 293T cells. After 2 weeks in culture, we purified genomic DNA (Qiagen). Standard curve for LV quantification was obtained from transduced 293T cells sorted for carrying one CpG. The CpG of genomic DNA standard curves and samples was determined using custom TaqMan assays specific for LVs (Applied Biosystems). LVs were injected i.v. at $2 \bullet 10^4$ ng p24/mouse in 50-200 µl depending on the infectivity.

Real-time quantitative PCR analysis and statistical analysis

Tumor nodules were visually identified and resected. Nodules were lysed with a mechanical rotor in lysis buffer. Total mRNA was purified following RNeasy Mini kit guidelines (QIAGEN). RNA was quantified and retrotranscribed with High-Capacity cDNA Reverse Transcription Kit (Thermo Fisher). Quantitative PCR analyses were performed with TaqMan assays from Applied Biosystems. Quantitative PCR was run for 40 cycles in standard mode using a StepOne apparatus (Applied Biosystems). The SDS software was used to extract raw data. The difference between the threshold cycle (CT) of each gene and that of the endogenous control 18S (ΔCT) was used to determine gene expression. Statistical testing was performed on fold-change values using 2-way ANOVA followed by Holm-Sidak multiple comparison test. P values were considered significant when < 0.05.

ELISA

PF4 levels in the supernatant of total liver cells were quantified by ELISA kit (R&D Systems) following the kit guidelines.

Flow cytometry

Spleens and bone marrow were minced into single-cell suspensions by mechanical dissociation. Lung tumors were minced into single-cell suspensions by enzymatic treatment as previously described (Pucci et al., 2009). Cell suspensions were stained with directly-conjugated antibodies (from Biolegend, BD or eBiosciences) and 7AAD (Sigma). Cells of interest were identified as shown in Fig. S2C or Fig. S3A. Eleven-color analyses were performed on a custom LSRII (BD) equipped with: 405nm laser and, in order, 450/50, 505LP, 515/20, 600LP, 610/20, 685LP, 695/40 filters; 488nm laser and, in order, 488/10, 505LP, 530/30, 550LP, 575/26, 685LP, 695/40 filters; 633nm laser and, in order, 660/20, 710LP, 730/45, 735LP, 780/60. Fluorochromes employed were, in order: BV421 or eFluor450, BV510, BV605, BV711, FITC or eGFP or eYFP, PE, 7AAD or PerCP-Cy5.5, PE-Cy7, APC, Alexa700, APC-Cy7 or APC-eFluor780.

Mouse Histology and Immunohistochemistry

For histological analysis of tumor burden in mice, lung tissues were harvested, formaldehyde-fixed and paraffin-embedded following standard procedures. Consecutive sections were prepared and stained with hematoxylin and eosin to define tumor tissue areas in the lung. Immunohistochemistry (IHC) on mouse tissue sections was performed as described previously (Pfirschke C, 2016). Briefly, mouse lung tumor sections were prepared and dried at 60°C for 1 h, dewaxed and rehydrated. We performed heat-induced epitope retrieval by incubating in 10 mM Tris (pH9.0) buffered solutions containing 0.05% Tween heated at 120°C for 2 min. To obtain consistent and reliable staining an automated staining system (LabVision Autostainer 360, Thermo Scientific) was used. To destroy all

endogenous peroxidase and alkaline phosphatase activity in the tissue, the sections were pretreated using BLOXALL endogenous enzyme-blocking solution (Vector Laboratories) for 10 min. After a blocking step with normal goat serum, the sections were incubated with the individual primary monoclonal antibody (mAb) for 1 h followed by secondary ImmPRESS polymer detection systems (Vector Laboratories) according to the manufacturers protocol. The DAB Plus Substrate System (Thermo Scientific) was applied as substrate and hematoxylin used for counterstain. Rat anti-mouse CD42b (clone Xia.G7, emfret Analytics) was used for staining mouse lung tumors and control tissues. Image documentation was performed using the NanoZoomer 2.0-RS slide scanner system (Hamamatsu) and CD42b positivity was identified using Fiji software.

Human Tumor Samples and Immunohistochemistry

Sections from paraffin-embedded biopsies of lung resections (n=29) from lung adenocarcinoma patients with known *KRAS* gene mutation status were obtained from the Department of Pathology at Massachusetts General Hospital. TP53 IHC was conducted with mAb clone DO-7 (Leica) as described previously (Pfirschke C, 2016). The following scoring system was used to assess *TP53* wild-type or mutational status (Köbel et al., 2010): score 0 (complete absence of staining: *TP53* null mutation); score 1 (focal nuclear expression in up to 50% of tumor cells: *TP53* wild-type); score 2 (nuclear overexpression in more than 50% of tumor cells: *TP53* missense mutation). Biopsies with scores 0 or 2 were categorized as *TP53* mutants and biopsies with score 1 as *TP53* wild-type. CD42b IHC was performed with an anti-human CD42b mAb (clone 42C01, Abcam) and CD42b positivity was identified using Fiji software.

Platelet-rich plasma (PRP) preparation and staining

PRP smears were analyzed to assess the specificity of the anti-human CD42b mAb (clone 42C01, Abcam). Human blood was collected in a vacuum tube containing anticoagulant and blood was centrifuged at 300 g for 15 min. Following centrifugation, 10 µl of the upper fraction, containing the PRP, was applied on a clean glass slide and a thin smear was prepared. After drying for 1 h the PRP smear was fixed in 4% formaldehyde-buffered solution and IHC performed as described above, omitting the heat-induced epitope retrieval. In addition, control staining with anti-human CD45 mAb (clone 2B11+PD7/26, DAKO) was performed to confirm that PRP was indeed depleted of leukocytes and to demonstrate the specificity of the CD42b mAb, which does not stain CD45+ leukocytes but only platelets.

Clopidogrel Treatment

Platelet inhibition was performed by daily i.p. injections of 10 mg/kg Clopidogrel (Quinn and Fitzgerald, 1999). Treatment was initiated 2 days before tumor challenge and for a duration of 5 weeks. KP1.9 cells ($2.5 \bullet 10^5$) were injected i.v.

Bioinformatics and Statistics

In silico analyses were performed in R. The initial list of murine candidates (i) used to probe lung cancer patient microarray datasets (ii) was sequentially transformed from a list of murine proteins into: 1) their human orthologs; 2) their gene symbol; 3) the corresponding microarray probe IDs. The list of microarray probes was then matched with human datasets for survival analysis, which used the log-rank test with Bonferroni correction. Such survival analysis consisted to operationally sort patients according to expression levels of each of the candidates, select high and low expressing patients (top and bottom 20%) and compare their overall survival. Unless otherwise specified, results were expressed as mean ± SEM. GraphPad Prism 6 was used for all statistical analyses. Statistical tests for multivariate analyses were performed using 2-way ANOVA followed by Holm-Sidak multiple comparison test. P values were considered significant when < 0.05.

Supplemental References

Cortez-Retamozo, V., Etzrodt, M., Newton, A., Rauch, P.J., Chudnovskiy, A., Berger, C., Ryan, R.J., Iwamoto, Y., Marinelli, B., Gorbatov, R., Forghani, R., Novobrantseva, T.I., Koteliansky, V., Figueiredo, J.L., Chen, J.W., Anderson, D.G., Nahrendorf, M., Swirski, F.K., Weissleder, R., and Pittet, M.J. (2012). Origins of tumor-associated macrophages and neutrophils. Proc Natl Acad Sci U S A *109*, 2491–2496.

De Palma, M., and Naldini, L. (2002). Transduction of a gene expression cassette using advanced generation lentiviral vectors. Methods Enzymol *346*, 514–529.

DuPage, M., Dooley, A.L., and Jacks, T. (2009). Conditional mouse lung cancer models using adenoviral or lentiviral delivery of Cre recombinase. Nat Protoc *4*, 1064–1072.

Köbel, M., Reuss, A., du Bois, A., Kommoss, S., Kommoss, F., Gao, D., Kalloger, S.E., Huntsman, D.G., and Gilks, C.B. (2010). The biological and clinical value of p53 expression in pelvic high-grade serous carcinomas. J Pathol *222*, 191–198.

Nguyen, D.X., Chiang, A.C., Zhang, X.H., Kim, J.Y., Kris, M.G., Ladanyi, M., Gerald, W.L., and Massagué, J. (2009). WNT/TCF signaling through LEF1 and HOXB9 mediates lung adenocarcinoma metastasis. Cell *138*, 51–62.

Pfirschke C, E.C., Rickelt S, Cortez-Retamozo V, Garris C, Pucci F, Yamazaki T, Poirier-Colame V, Newton A, Redouane Y, Lin YJ, Wojtkiewicz G, Iwamoto Y, Mino-Kenudson M, Huynh TG, Hynes RO, Freeman GJ, Kroemer G, Zitvogel L, Weissleder R, Pittet MJ (2016). Immunogenic Chemotherapy Sensitizes Tumors to Checkpoint Blockade Therapy. Immunity *44*, p343–p354.

Pucci, F., Venneri, M.A., Biziato, D., Nonis, A., Moi, D., Sica, A., Di Serio, C., Naldini, L., and De Palma, M. (2009). A distinguishing gene signature shared by tumor-infiltrating Tie2-expressing monocytes, blood “resident” monocytes, and embryonic macrophages suggests common functions and developmental relationships. Blood *114*, 901–914.

Quinn, M.J., and Fitzgerald, D.J. (1999). Ticlopidine and clopidogrel. Circulation 100, 1667–1672

Taguchi, A., Politi, K., Pitteri, S.J., Lockwood, W.W., Faca, V.M., Kelly-Spratt, K., Wong, C.H., Zhang, Q., Chin, A., Park, K.S., Goodman, G., Gazdar, A.F., Sage, J., Dinulescu, D.M., Kucherlapati, R., Depinho, R.A., Kemp, C.J., Varmus, H.E., and Hanash, S.M. (2011). Lung cancer signatures in plasma based on proteome profiling of mouse tumor models. Cancer Cell *20*, 289–299.